Thank you very much again for your quick and thoughtful feedback on our response. Since this response includes several figures, we would appreciate it if you could read the attached PDF version.

>> all events discussed by Partamies et al. (2025) are dayside cases observed at Svalbard

This is not entirely true because their event in Figure 14c is on the nightside (19 MLT). Figure 14c shows picket fence-like emissions. I'm not sure why Svalbard vs. Scandinavia can claim the uniqueness of the paper. Both papers show observations near the poleward edge of the auroral oval, providing a similar geophysical context. The latitude is different, but the oval location changes with magnetic activity. Considering these, I still urge that the observations by Partamies et al. (2025) should be introduced and acknowledged. Although the point of your paper is the nightside observations, the common nature of the emissions near the poleward edge of the oval should be stated clearly.

Thank you for pointing this out. You are right that Partamies et al. (2025) present an event around 19 MLT. We had overlooked this case and therefore incorrectly summarized their study as dealing only with dayside events from Svalbard. We will correct this in the revised manuscript.

We also agree that, once the shift of the auroral oval with geomagnetic activity is taken into account, the distinction between Svalbard and northern Scandinavia alone does not by itself provide scientific uniqueness. Partamies et al. (2025) is an important prior work for our study, and, as you point out, some of their findings overlap with our results in that they show similar emissions near the poleward edge of the auroral oval.

At the same time, our observations are not entirely overlapping with theirs. For example, by using a high-spatiotemporal-resolution camera, we are able to resolve additional morphological characteristics of the structures (e.g., their small-scale spacing, temporal evolution, and relation to the background auroras) that were not analyzed in detail in Partamies et al. (2025), since these features were not the main focus of their study. These differences are not intended to suggest any inconsistency or error in Partamies et al. (2025); rather, we see our analysis as complementary to theirs, adding higher-resolution morphological details of green emissions. In the revised manuscript, we will introduce and acknowledge their results more clearly, and explicitly state both the common nature of the emissions occurring near the poleward edge of the oval and how our observations extend their work.

> I don't think that revised Figure 5 demonstrates this point. I have copied my markups to revised Figure 5 (see the PDF version of the comment). My previous comment pointed out that a significant part of the picket fence is not field aligned, and this version of the figure still shows the same issue. Although I agree that the orientation tracks the changes of field line orientation overall, the misalignment of a significant part of the picket fence does not support the conclusion that the picket fence for Event 1 is field-aligned.

Thank you for your comment. Following your suggestion, we attempted to quantitatively evaluate the deviation between the observed FAE inclination and the modeled magnetic field-line inclination. The detailed analysis procedure will be included in the main manuscript as an appendix in the formal revision.

As a result, we were able to automatically extract 26 FAE structures, and the absolute difference between their inclinations and those of the modeled magnetic field lines was found to be 5.23° in mean and 4.01° in standard deviation.

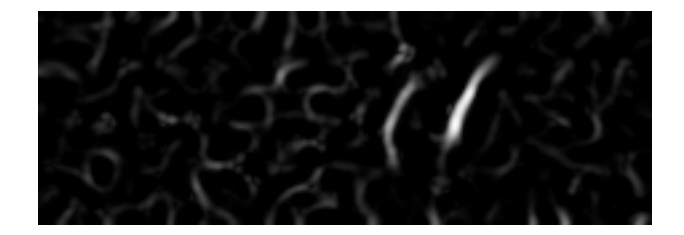
As discussed below, these values naturally arise when we consider the combined uncertainties associated with the linear fitting of the FAE, possible errors in the magnetic field model itself, and the uncertainty in the qCMOS camera's geometrical calibration. Therefore, it is statistically difficult to conclude that "the FAE inclination is systematically different from the inclination of the model magnetic field line." As we noted in our previous response, although the spatial alignment between the two is not perfect, we do not have sufficient grounds to claim a significant departure of FAE inclination from the model field-line direction. Rather, we believe that the FAE orientation is fundamentally aligned with the magnetic field, consistent with our previous reply. Nevertheless, to avoid emphasizing perfect agreement (i.e., that both angles should be exactly 0° everywhere), we will revise the text to make the interpretation clearer and more transparent.

Outline of the analysis

- (1) Extraction of each FAE
- (2) Fitting the extracted structure with a line and computing its inclination on the image
- (3) Computing the model magnetic field inclination in the image and interpolating to all pixels
- (4) Comparing the inclinations obtained in (2) and (3) and evaluating the mean and scatter of the differences

(1)

We processed each image in the interval shown in Figure 5 individually. From each original observational image, we extracted the region of interest (ROI) where the FAE appeared (x = 450-680 pix, y = 160-240 pix). The FAE observed in this event was faint, with 16-bit pixel values typically ranging from 3150 to 3700. Because this intensity range is close to the background noise level, simple thresholding failed to reliably identify filamentary structures. Therefore, we normalized the ROI using the 5–95 percentile range (to suppress the influence of bright stars), and applied the Frangi vesselness filter, which is designed to enhance elongated structures such as blood vessels (Frangi et al., 1998). The resulting Frangi response image applied to Figure 5d is shown below.



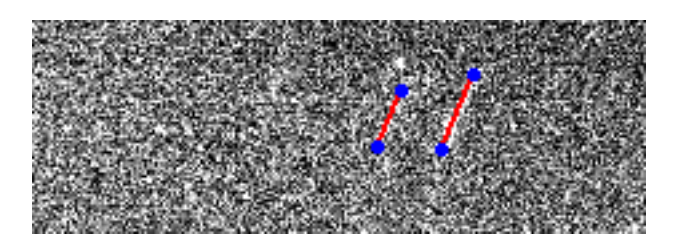
As seen in the figure, two elongated structures are clearly enhanced on the right in the middle of the image. We selected the top 1% of pixels in the Frangi response as initial FAE candidates. Among these, we retained only those pixels whose original intensities lay within 3150–3700, and removed candidate regions with an area smaller than 45 pixels. The resulting binary mask is shown below.



From these candidate regions, only those with eccentricity greater than 0.8 were considered true FAE structures. In the example shown, both regions met this criterion.

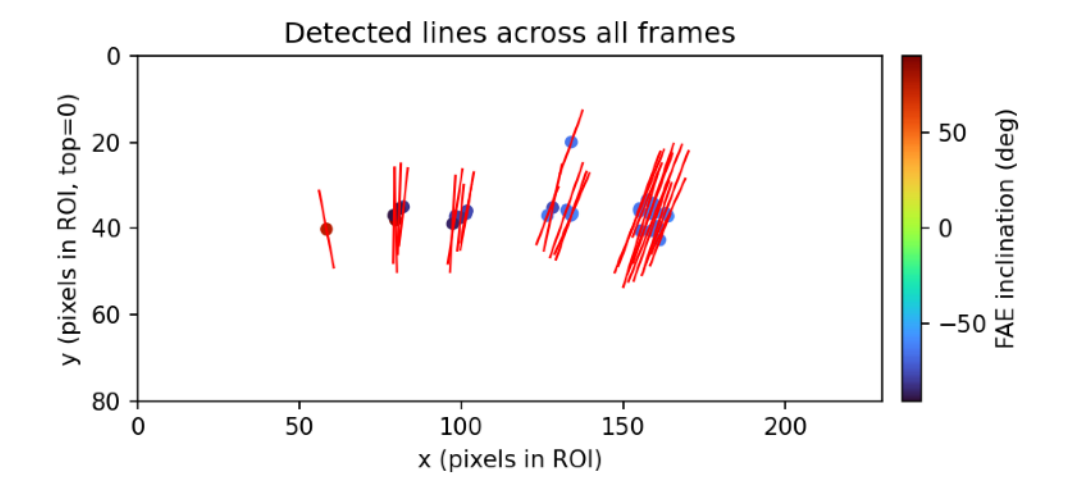
(2)

For each accepted region, we collected all pixel coordinates and computed their centroid. We then applied principal component analysis (PCA) to determine the dominant elongation direction. By projecting each pixel onto the first principal component, we identified the minimum and maximum projection values, and defined the corresponding positions along the PCA axis as the endpoints of the fitted line segment. Thus, each FAE was represented by a single straight line defined by these two endpoints. An example result is shown below, where the red line indicates the fitted segment and the blue points mark its endpoints.

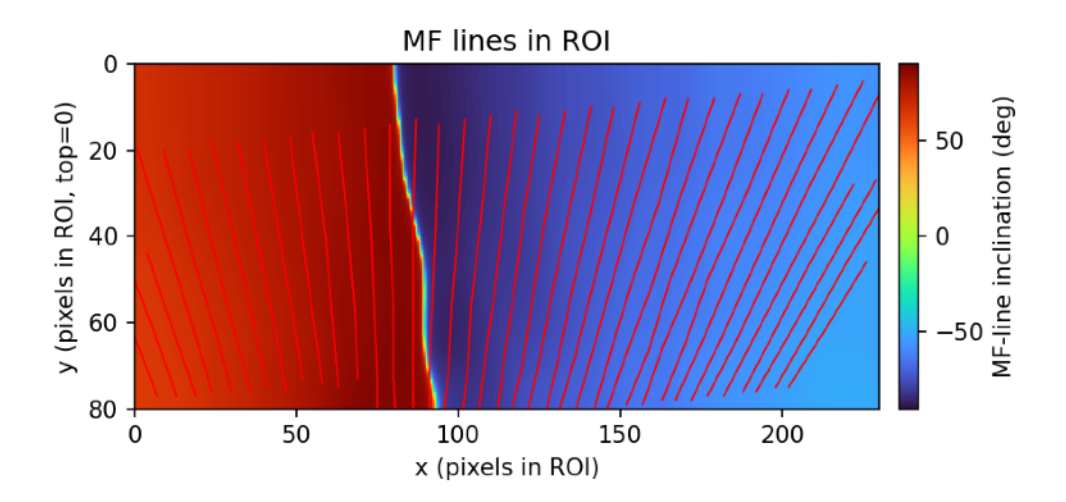


Although the background image appears noisy, this is because it was generated only for debugging (scaled to 8-bit using the 5–95 percentile range). The fitting in step (2) does not use this background image.

Repeating this procedure for all frames in the interval produced 26 line segments in total. These segments were plotted together in the ROI coordinate system, with the inclination of each segment indicated by a colored dot placed at its midpoint (figure below).



We further traced the magnetic field lines shown as yellow dots in revised Figure 5, using a finer latitude sampling (0.05° step). For each pair of consecutive field-line points, we computed the local inclination in the image using $\theta = \arctan 2(\Delta y, \Delta x)$, where Δx and Δy denote the pixel-coordinate differences between two adjacent field-line points. We interpolated these inclination values over the entire ROI using Gaussian filtering so that every pixel has an estimated inclination. The resulting inclination field is shown below; the red curves show the model magnetic field lines and the background color represents the local inclination.



With this, we were able to directly compare the observed FAE inclination with the modeled field-line inclination at the same locations.

(4) For the 26 detected structures, the absolute difference $|\Delta\theta|$ between the observed FAE inclination and the modeled magnetic field-line inclination was computed. The results are:

Number of extracted segments: 26

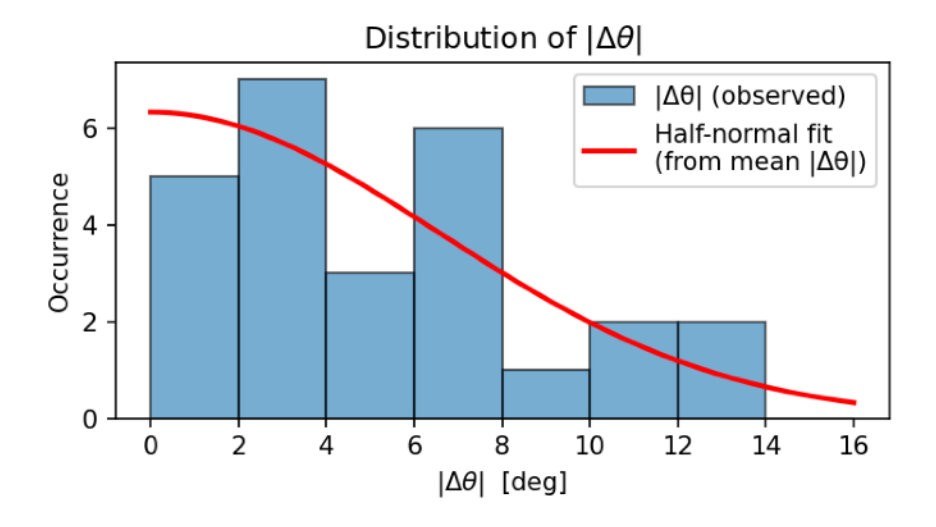
Mean $|\Delta\theta|$: 5.23 (deg)

Standard deviation $|\Delta\theta|$: 4.01 (deg)

The distribution of $|\Delta\theta|$ is shown in the histogram below. For reference, we superimposed the half-normal probability density function derived from the observed mean value (the vertical scale is multiplied by a constant for clarity). Although the sample size is small and the histogram does not perfectly match the curve, the following qualitative features are consistent:

- (a) Many samples (12; 46% of all) lie within 0-4°, and
- (b) the frequency decreases for values above 8°, producing a natural long tail.

Thus, the observed distribution is broadly consistent with a half-normal distribution.



To interpret the mean and standard deviation, we model the observed inclination difference as

$$\Delta \theta_{\text{obs},i} = \theta_{\text{FAE},i} - \theta_{\text{MF},i} = \Delta \theta_{\text{true}} + \varepsilon_i, \qquad \varepsilon_i \sim \mathcal{N}(0,\sigma^2),$$

where ε_i represents the combined uncertainty from the linear fitting of the segments, magnetic field-line modeling, and geometrical calibration of the observed image. Assuming that the FAE is intrinsically parallel to the true magnetic field in the image, we set $\Delta\theta_{\rm true}=0$, giving

$$\Delta \theta_{\text{obs}\,i} = \varepsilon_i$$
.

The absolute value $X = |\varepsilon_i|$ then follows a half-normal distribution with

$$\mathbb{E}[X] = \sigma \sqrt{\frac{2}{\pi}}, \quad \operatorname{Var}(X) = \sigma^2 \left(1 - \frac{2}{\pi}\right).$$

Using the observed mean value $\overline{|\Delta\theta|} = 5.24^{\circ}$, we estimate 1σ uncertainty in $\Delta\theta_{{\rm obs},i}$ as

$$\hat{\sigma} = \overline{|\Delta\theta|} \sqrt{\frac{\pi}{2}} \approx 5.24^{\circ} \times \sqrt{\frac{\pi}{2}} \approx 6.6^{\circ}.$$

The predicted standard deviation of $|\Delta\theta|$ is then

$$\sqrt{\text{Var}(|\Delta\theta_{\text{obs}}|)} = \hat{\sigma}\sqrt{1 - \frac{2}{\pi}} \approx 6.6^{\circ} \times \sqrt{1 - \frac{2}{\pi}} \approx 4.0^{\circ},$$

which agrees very well with the observed value of 4.01°.

Thus, the observed $|\Delta\theta|$ values are fully consistent with the hypothesis that the FAE is intrinsically parallel to the magnetic field in the image, and that the measured deviation simply reflects the combined 1σ uncertainty of 6–7° arising from the linear fitting of segments and geometrical/model errors. Therefore, it is statistically difficult to conclude that "the FAE inclination is systematically different from the model magnetic field line," and the present results are more naturally explained if the FAE orientation is regarded as parallel to the magnetic field within the observational and modeling uncertainties.

Reference:

Frangi, A.F., Niessen, W.J., Vincken, K.L., Viergever, M.A. (1998). Multiscale vessel enhancement filtering. In: Wells, W.M., Colchester, A., Delp, S. (eds) Medical Image Computing and Computer-Assisted Intervention — MICCAI'98. MICCAI 1998. Lecture Notes in Computer Science, vol 1496. Springer, Berlin, Heidelberg. https://doi.org/10.1007/BFb0056195